Langmuir

Article

pubs.acs.org/Langmuir

Emergence of a Stern Layer from the Incorporation of Hydration Interactions into the Gouy−Chapman Model of the Electrical Double Layer

Matthew A. Brown,[†] Guilherme Volpe Bossa,[‡] and Sylvio May*[,‡]

[†]Laboratory for Surface Science and Technology, Department of Materials, ETH Zürich, CH-8093 Zurich, Switzerland

[‡]Department of Physics, North Dakota State University P.O. Box 6050, Fargo, North Dakota 58108-6050, United States

ABSTRACT: In one of the most commonly used phenomenological descriptions of the electrical double layer, a charged solid surface and a diffuse region of mobile ions are separated from each other by a thin charge-depleted Stern layer. The Stern layer acts as a capacitor that improves the classical Gouy−Chapman model by increasing the magnitude of the surface potential and limiting the maximal counterion concentration. We show that very similar Stern-like properties of the diffuse double layer emerge naturally from adding a nonelectrostatic hydration repulsion to the electrostatic Coulomb potential. The interplay of electrostatic attraction and hydration repulsion of the counterions and the surface leads to the formation of a diffuse counterion layer that remains well separated from the surface. In addition, hydration repulsions between the ions limit and control the maximal ion concentration and widen the width of the diffuse double layer. Our mean-field model, which we express in terms of electrostatic and hydration potentials, is physically consistent and conceptually similar to the classical Gouy−Chapman model. It allows the incorporation of ion specificity, accounts for hydration properties of charged surfaces, and predicts Stern layer properties, which we analyze in terms of the effective size of the hydrated counterions.

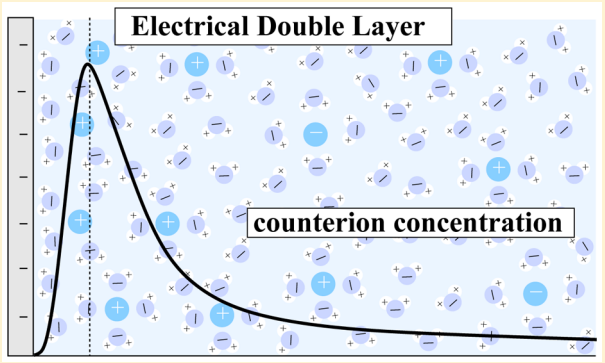

INTRODUCTION

It is generally accepted that the specific nature of the electrolyte ions in aqueous solutions plays a vital role in dictating the electrical properties of charged interfaces. Both the surface charge densities[1,2] and the electrical potentials[3,4] regularly depend on the identity of the co- and counterions in the electrolyte solution. These general observations are often termed specific ion effects,[5,6] and their ramifications are, for example, evident in colloidal[7] and biological[8] settings. The microscopic origins of specific ion effects are, however, complex and poorly understood and therefore continue to fascinate the experimental and theoretical communities alike.

There exist several different models for the structure of the electrical double layer (EDL), but the Gouy−Chapman−Stern (GCS) model[9] has proved most successful in fitting experimental results for a variety of different solid−electrolyte interfaces.[10,11] The GCS model is an elementary extension of the Gouy−Chapman (GC) model that inserts a Helmholtz capacitor of thickness d_{Stern}, termed the Stern layer, between the charged surface and the diffuse ion cloud.[12] Because no electrolyte ions reside within d_{Stern}, the potential drop to the surface is like that of a capacitor (a linear function in the case of a smooth planar surface). Outside the Stern layer the potential profile and ion distributions of the GCS model are given by the solution of the classical Poisson−Boltzmann equation. The combination of capacitor and diffuse layer regions in the GCS model results in an (often substantial) increase of the predicted magnitude of the surface potential relative to models that have only one or the other.

From a theoretical standpoint the Stern layer does not emerge naturally from the solution of the classical Poisson−Boltzmann equation but appears after accounting for the finite sizes of the ions in the electrolyte through excluded volume interactions.[13−17] This places the charge of each ion at the center of a sphere of well-defined radius, typically chosen to match the hydrated ion size. The finite-size modification limits the concentration of counterions near the surface, an obvious improvement over the solution of the classical Poisson−Boltzmann equation, while at the same time creating a thin, charge-depleted region close to the surface. The width of this uncharged region is set by the imposed excluded volume potential and is equal to d_{Stern}. Computer simulations suggest, however, that the nonelectrostatic contributions to the ion−ion interaction potentials in aqueous solutions are *soft* and decay over the length scale of a few water molecules[18] and are therefore not best modeled by the hard-core potential of the excluded volume interaction. A few attempts have been made to incorporate additional soft interaction potentials into the

Received: June 30, 2015
Revised: August 30, 2015
Published: October 16, 2015

DOI: 10.1021/acs.langmuir.5b02389
Langmuir 2015, 31, 11477−11483

Gouy–Chapman model,[19−22] but the predictions were not analyzed in terms of Stern layer formation.

In the approach put forward here the nonelectrostatic interactions of the counterions with the charged surface, and that between the counterions themselves, are modeled as soft interactions, namely repulsive Yukawa potentials that mimic the structural forces due to ion- and surface-induced hydration effects.[23] We describe these hydration-mediated interactions on the same level as the electrostatic interactions by introducing a hydration potential in addition to the electrostatic potential. Our approach, which retains the conceptual simplicity of the GC model, yields properties reminiscent of the Stern layer, with a charge-depleted region and corresponding linear behavior of the electrostatic potential. In addition, the interionic hydration repulsion limits the counterion concentration close to the surface. The maximal value of the counterion concentration close to the surface reflects the packing of the counterions including their hydration shells: it decreases with the effective counterion size but remains largely independent of the bulk salt concentration.

THEORY

Consider a planar solid surface with a fixed, uniform, and sufficiently high negative surface charge density σ_e. The surface is in contact with an aqueous solution containing a symmetric 1:1 electrolyte of bulk concentration n_0. The electrostatic potential in the aqueous solution, $\Phi(x)$, at distance x away from the surface fulfills the Poisson equation $\epsilon_W\epsilon_0\Phi''(x) = -\rho(x)$, where a prime denotes the derivative with respect to the argument; $\epsilon_0 = 8.85 \times 10^{-12}$ F/m is the permittivity of free space and $\epsilon_W = 78$ the dielectric constant of water. The local volume charge density within the electrolyte $\rho(x) = e[n_+(x) - n_-(x)]$ reflects the difference of concentrations between mobile electrolyte cations (n_+) and anions (n_-); the elementary charge is $e = 1.6 \times 10^{-19}$ C. It is common to re-express the Poisson equation

$$\Psi_e''(x) = -4\pi l_e[n_+(x) - n_-(x)] \tag{1}$$

in terms of the dimensionless electrostatic potential $\Psi_e = e\Phi/k_BT = \Phi/(25\text{ mV})$ and the Bjerrum length in water $l_e = e^2/(4\pi\epsilon_W\epsilon_0 k_BT) = 0.7$ nm, where k_B is the Boltzmann constant and $T = 300$ K the absolute temperature. The classical GC model combines the Poisson equation with Boltzmann distributions for the local ion concentrations, $n_+ = n_0 e^{-\Psi_e}$ and $n_- = n_0 e^{\Psi_e}$, yielding the classical Poisson–Boltzmann equation $\Psi_e''(x) = \kappa_e^2 \sinh[\Psi_e(x)]$ with

$$\kappa_e^2 = 8\pi l_e n_0 \tag{2}$$

The length $1/\kappa_e$ is known as the Debye screening length.[24] We point out that the Poisson equation expresses interactions through the Coulomb potential with electrostatic energies $U_e/k_BT = l_e/r$ and $U_e/k_BT = -l_e/r$ between elementary charges of the same and different signs, respectively, that are separated by a distance r. Consequently, the classical GC model accounts only for purely electrostatic ion–ion and ion–surface interactions.

Ions and surfaces induce water molecules to form hydration shells, which mediate hydration interactions.[25−27] A negatively charged surface attracts mobile cations (the counterions) that reside in close proximity at elevated concentrations as compared to the bulk, whereas the mobile anions (the co-ions) are depleted from the surface. Hence, close to a highly negatively charged surface we expect hydration interactions to be relevant for the mobile cations and negligible for the mobile anions. To model these interactions, we assume cations to produce not only an electrostatic but also an additional hydration interaction that we model as a Yukawa potential $U_h/k_BT = e^{\kappa(l_h-r)}l_h/r$, where $1/\kappa = 0.3$ nm is the decay length of the ordered water layers[25] and r the distance between two cations. The length l_h denotes the ion-to-ion separation at which the hydration interaction is equal to the thermal energy unit k_BT. Hence, we expect l_h reflects the effective ion size, namely the crystallographic size plus the thickness of a soft hydration shell.[28] The choice of a Yukawa-like interaction $\sim e^{-\kappa r}/r$ is motivated by a phenomenological model of hydration forces due to Marcelja and Radic[23] and ensures the cations remain fully hydrated near the charged surface. Detailed molecular dynamics (MD) simulations[29−31] and continuum solvation models[32] predict a similar decay, yet with an additional oscillatory component that under specific conditions would allow cations near the charged surface to get trapped in a local minimum state that may involve (partial) dehydration and the formation of an inner-sphere complex. The inclusion of an oscillatory component into the present model is possible but mathematically more involved. For this reason we have omitted its inclusion in the present work. Hence, the total cation–cation interaction energy in our model is

$$\frac{U_{tot}}{k_BT} = \frac{U_e}{k_BT} + \frac{U_h}{k_BT} = \frac{l_e}{r} + \frac{l_h}{r}e^{\kappa(l_h-r)} \tag{3}$$

whereas cation–anion and anion–anion interactions remain purely Coulombic ($U_{tot}/k_BT = l_e/r$ for the anion–anion interaction and $U_{tot}/k_BT = -l_e/r$ for the cation–anion interaction). Here we note again that there is no need to include hydration interactions involving the anions as long as their local concentration is sufficiently small everywhere in the aqueous solution. Figure 1 shows the cation–cation interaction energy $U_{tot}(r)/k_BT$ for $l_h = 0.2$ nm (black solid line), $l_h = 0.4$ nm (blue line), $l_h = 0.6$ nm (red line), and $l_h = 0.8$ nm (green line). These are the values on which our analysis in the Results and Discussion section will focus. The first three of these effective cation sizes are representative of the hydrated alkali

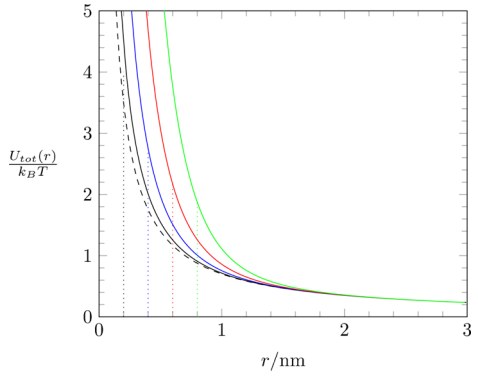

Figure 1. Total cation–cation interaction energy $U_{tot}(r)$ according to eq 3 with $l_e = 0.7$ nm and $\kappa^{-1} = 0.3$ nm. The different solid lines correspond to $l_h = 0.2$ nm (black), $l_h = 0.4$ nm (blue), $l_h = 0.6$ nm (red), and $l_h = 0.8$ nm (green). At these values for l_h (marked by dotted vertical lines) the hydration interaction energy $U_h(r = l_h)$ equals the thermal energy k_BT. The dashed line shows the electrostatic contribution $U_e/k_BT = l_e/r$.

DOI: 10.1021/acs.langmuir.5b02389
Langmuir 2015, 31, 11477−11483

metal cations[28] (Cs^+_{hyd} ~ 0.2 nm, Na^+_{hyd} ~ 0.4 nm, and Li^+_{hyd} ~ 0.6 nm).

Similar to translating the Coulomb interaction $U_e/k_BT = \pm l_e/r$ between two ions to the Poisson equation for the associated dimensionless electrostatic potential Ψ_e in eq 1, we can also translate the hydration interaction $U_h/k_BT = e^{\kappa(l_h - r)} l_h/r$ to a local differential equation for an associated (dimensionless) hydration potential $\Psi_h(x)$. The result is the inhomogeneous Helmholtz equation[22]

$$\Psi_h''(x) - \kappa^2 \Psi_h(x) = -4\pi l_h e^{\kappa l_h}[n_+(x) - n_0] \tag{4}$$

Equation 4 does not contain n_-; this is a consequence of focusing exclusively on hydration interactions between cations (counterions) in the aqueous solution. The local cation and anion concentrations fulfill Boltzmann distributions

$$n_+(x) = n_0 e^{-\Psi_e(x) - \Psi_h(x)}, \qquad n_-(x) = n_0 e^{\Psi_e(x)} \tag{5}$$

where, again, the hydration potential $\Psi_h(x)$ is only associated with the mobile cations. The Boltzmann distributions in eq 5 can be derived rigorously by minimizing an appropriate mean-field free energy functional.[22]

Inserting the Boltzmann distributions into eqs 1 and 4 yields two second-order, coupled differential equations for the two fields $\Psi_e(x)$ and $\Psi_h(x)$

$$\Psi_e''(x) = \frac{\kappa_e^2}{2}[e^{\Psi_e(x)} - e^{-\Psi_e(x) - \Psi_h(x)}]$$

$$\Psi_h''(x) - \kappa^2 \Psi_h(x) = \frac{\kappa_h^2}{2}[1 - e^{-\Psi_e(x) - \Psi_h(x)}] \tag{6}$$

where κ_e (the inverse of the Debye screening length) is defined in eq 2 and

$$\kappa_h^2 = 8\pi l_h e^{\kappa l_h} n_0 \tag{7}$$

In the absence of the hydration potential, we identify the first line in eqs 6 as the classical Poisson–Boltzmann equation. Prior to solving the coupled system in eqs 6, we need to specify four boundary conditions. Two of them

$$\Psi_e'(0) = -4\pi l_e \frac{\sigma_e}{e}, \qquad \Psi_h'(0) = -4\pi l_h e^{\kappa l_h} \sigma_h \tag{8}$$

reflect the surface charge density σ_e and the density of sources for the hydration interaction of the cations with the surface, respectively. Regarding the latter, each ordered water molecule on the surface can be expected to act as a source; a reasonable choice is therefore the surface density of water molecules σ_h = 5/nm^2. The remaining two boundary conditions, $\Psi_e(x \to \infty) = 0$ and $\Psi_h(x \to \infty) = 0$, render the surface to be isolated. We treat the two parameters κ^{-1} = 0.3 nm and σ_h = 5/nm^2 as fixed constants throughout this work. (However, this does not exclude them from being adjusted in order to fit experimental data.)

The two coupled second-order differential equations for $\Psi_e(x)$ and $\Psi_h(x)$, specified in eqs 6, can be solved numerically by employing a Newton–Raphson iteration procedure. To this end, the two nonlinear equations are re-expressed as two linear second-order differential equations

$$\frac{2}{\kappa_e^2}\Psi_e'' = (e^{\tilde{\Psi}_e} + e^{-\tilde{\Psi}_e - \tilde{\Psi}_h})(\Psi_e - \tilde{\Psi}_e) + e^{-\tilde{\Psi}_e - \tilde{\Psi}_h}(\Psi_h - \tilde{\Psi}_h) + e^{\tilde{\Psi}_e} - e^{-\tilde{\Psi}_e - \tilde{\Psi}_h}$$

$$\frac{2}{\kappa_h^2}(\Psi_h'' - \kappa^2 \Psi_h) = e^{-\tilde{\Psi}_e - \tilde{\Psi}_h}(\Psi_e - \tilde{\Psi}_e + \Psi_h - \tilde{\Psi}_h) + 1 - e^{-\tilde{\Psi}_e - \tilde{\Psi}_h} \tag{9}$$

whose solutions $\Psi_e(x)$ and $\Psi_h(x)$ are used as input $\tilde{\Psi}_e$ and $\tilde{\Psi}_h$ for the next iteration. Convenient starting functions are $\tilde{\Psi}_e = \tilde{\Psi}_h = 0$. Once the solutions have become stationary, $\Psi_e(x) = \tilde{\Psi}_e(x)$ and $\Psi_h(x) = \tilde{\Psi}_h(x)$, the nonlinear system is solved. The computational effort to solve eqs 9 is marginal and, in fact, comparable to numerically solving the classical Poisson–Boltzmann equation.

RESULTS AND DISCUSSION

The combination of electrostatic and hydration-mediated interactions in the EDL can lead to structural properties similar to the Stern layer extension of the GC model. We illustrate this behavior by presenting in Figure 2 the potentials $\Psi_e(x)$ and $\Psi_h(x)$ (upper diagram) as well as $n_+(x)$ and $n_-(x)$ (lower diagram), derived for κ^{-1} = 0.3 nm, $\sigma_e/e = -1/\text{nm}^2$, σ_h = 5/nm^2, and κ_e^{-1} = 1 nm. The four solid lines in each diagram (and

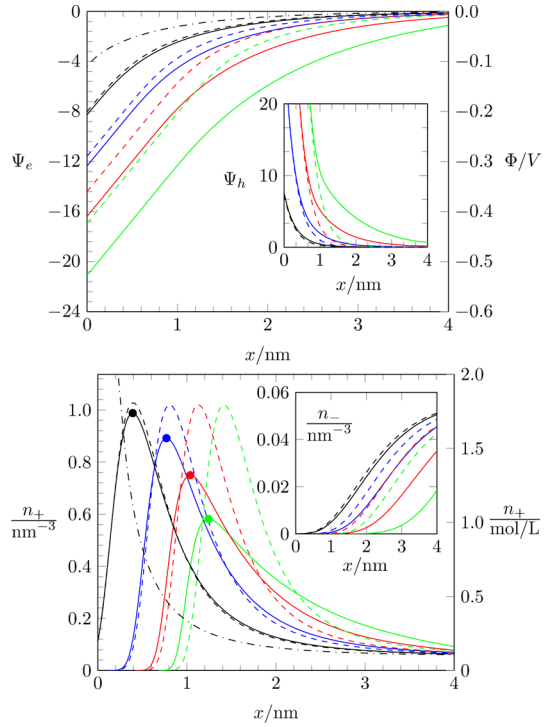

Figure 2. $\Psi_e(x)$ and $\Psi_h(x)$ (upper diagram), and $n_+(x)$ and $n_-(x)$ (lower diagram). Different curves correspond to different hydration repulsion strengths: l_h = 0.2 nm (black), l_h = 0.4 nm (blue), l_h = 0.6 nm (red), l_h = 0.8 nm (green). The solid lines account for cation–cation hydration repulsion whereas the dashed lines ignore it. The dashed lines in the inset of the upper diagram follow eq 10. The filled circles in the lower diagram mark the maximum counterion concentration $n_+(d_{Stern})$ at position d_{Stern}. The black dash-dotted line corresponds to the electrostatic potential (upper diagram) and counterion concentration (lower diagram) according to the classical GC model. All results are derived for fixed κ^{-1} = 0.3 nm, $\sigma_e/e = -1/\text{nm}^2$, σ_h = 5/nm^2, and κ_e^{-1} = 1 nm. The Debye screening length κ_e^{-1} = 1 nm corresponds to a bulk salt concentration of n_0 = 0.1 M = 0.057/nm^3; for large x all curves in the lower diagram (including the inset) converge to this value.

DOI: 10.1021/acs.langmuir.5b02389
Langmuir 2015, 31, 11477–11483

the insets) correspond to l_h = 0.2 nm (black), l_h = 0.4 nm (blue), l_h = 0.6 nm (red), and l_h = 0.8 nm (green).

Figure 2 is a manifestation of Stern-like EDL properties: Each electrostatic potential $\Phi(x) = \Psi_e(x) \times 0.025$ V (solid lines in the upper diagram) exhibits linear behavior within a region $0 \leq x \lesssim d_{\text{Stern}}$ of the charged surface, prior to decaying to zero. Both the magnitude of the surface potential $\Phi(0)$ and the width d_{Stern} of the linear region grow with the effective counterion size l_h. (Recall that l_h is the distance at which the hydration repulsion equals the thermal energy k_BT.) The linearity of $\Phi(x)$ suggests to identify the region from the surface to d_{Stern} as a Stern layer. Consistent with this notion, the counterion concentrations (lower diagram in Figure 2) adopt their maximum value $n_+(d_{\text{Stern}})$ at the Stern plane $x = d_{\text{Stern}}$, whereas counterions (and co-ions, see inset) are depleted from within the Stern layer, $x \lesssim d_{\text{Stern}}$. The locations d_{Stern} and $n_+(d_{\text{Stern}})$ are marked by a filled circle in the lower diagram of Figure 2. We also note that unlike the classical Gouy–Chapman model for point-like ions, the addition of a hydration repulsion confines the maximal counterion concentrations $n_+(d_{\text{Stern}})$ to physically reasonable values. For a surface charge density $\sigma_e/e = -1/\text{nm}^2$ and a 0.1 M bulk salt concentration (which implies a Debye screening length κ_e^{-1} = 1 nm) the classical Gouy–Chapman model (see the dash-dotted lines in Figure 2) predicts a surface potential of $\Phi_e(0) = -110$ mV and a corresponding counterion concentration of 8 M at the surface. In contrast, with the hydration repulsion included we find maximal counterion concentrations $n_+(d_{\text{Stern}})$ in the range of 1–2 M. We also make the physically reasonable observation that a larger effective ion size (growing l_h) results in decreasing $n_+(d_{\text{Stern}})$. If we again reference the hydrated alkali metal cations, to which our values of l_h are most directly compared,[28] this result is directly supported by experiment.[3]

To obtain a better physical understanding of how hydration interactions affect EDL properties, we switch off the mutual hydration repulsion between cations while retaining the hydration repulsion of the cations with the surface. Mathematically this is accomplished by setting the right-hand side of the second equation of eqs 6 to zero, yielding $\Psi_h''(x) - \kappa^2\Psi_h(x) = 0$, while keeping the boundary condition for the hydration potential Ψ_h in eq 8. We obtain the simple exponential decay

$$\Psi_h(x) = \frac{4\pi l_h \sigma_h}{\kappa} e^{\kappa(l_h - x)} \tag{10}$$

which enters the Boltzmann distribution of the counterions $n_+(x)$ in eq 5 as a fixed potential. Hence, counterions interact with the charged surface not only electrostatically but also via the external, surface-generated hydration potential in eq 10. A related approach of incorporating ion–surface hydration forces, mediated through dielectric saturation, was developed by Gur et al.[33] The predictions of the model based on eq 10 are shown in Figure 2 as dashed lines. Solid and dashed lines of the same color correspond to respectively including and ignoring cation–cation hydration repulsion for fixed effective cation size (fixed l_h). The dashed lines in the inset of the upper diagram in Figure 2 correspond to $\Psi_h(x)$ according to eq 10. Recall that a more positive hydration potential $\Psi_h(x)$ reduces the local counterion concentration $n_+ = n_0 e^{-\Psi_e - \Psi_h}$. Indeed, close to the surface $\Psi_h(x)$ adopts large positive values. Without accounting for cation–cation hydration repulsion, $\Psi_h(x)$ originates only from the surface and decays exponentially. With cation–cation hydration repulsion being present, $\Psi_h(x)$ develops an additional tail that extends further into the EDL (solid lines in the inset of the upper diagram) and thus decreases the counterion concentration even more. This decrease is more pronounced for larger effective cation sizes l_h. We contrast this to the absence of cation–cation hydration repulsion, where a Stern layer still forms but the maximal counterion concentration $n_+(d_{\text{Stern}})$ remains unaffected by the counterion size, a finding that is physically unreasonable. This highlights the importance of accounting for hydration interactions of counterions not only with the surface but also among each other.

Varying the salt concentration in the bulk of the aqueous solution affects the Debye screening length and thus the diffuse part of the EDL but has virtually no effect on the counterion concentration profile close to the Stern layer. This is illustrated in Figure 3 for fixed κ^{-1} = 0.3 nm, $\sigma_e/e = -1/\text{nm}^2$, $\sigma_h = 5/\text{nm}^2$,

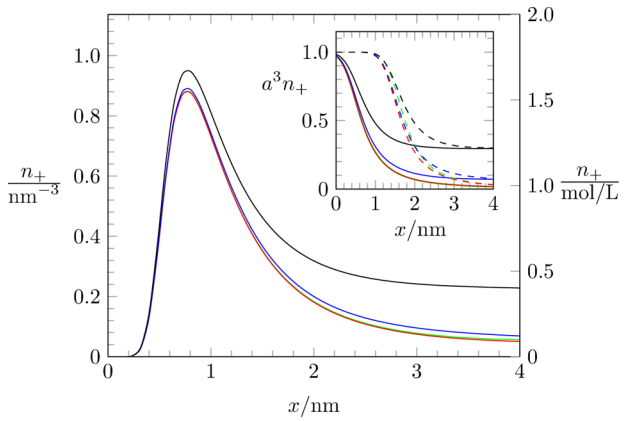

Figure 3. Counterion concentration profile $n_+(x)$ for κ^{-1} = 0.3 nm, $\sigma_e/e = -1/\text{nm}^2$, $\sigma_h = 5/\text{nm}^2$, and l_h = 0.4 nm. Different curves correspond to different salt concentrations in the bulk: n_0 = 1 mM (red), 4 mM (green), 100 mM (blue), and 400 mM (black). The inset shows predictions of the lattice gas GC model with a cell size of $a = 2\ l_h$ = 0.8 nm according to eq 11 for the same set of salt concentrations as in the main diagram. Solid and dashed lines in the inset correspond to $\sigma_e/e = -1/\text{nm}^2$ and $\sigma_e/e = -2/\text{nm}^2$, respectively.

and l_h = 0.4 nm. Different curves correspond to different salt concentrations in the bulk: 1 mM (red), 4 mM (green), 100 mM (blue), and 400 mM (black).

Saturation of the counterion concentration due to steric (that is excluded volume) repulsion is predicted by various recent models.[17,34−36] One prominent example is to replace the ideal gas that forms the basis of the classical GC model by a lattice gas with a cell volume a^3 that represents the effective (including a hydration shell of fixed extension) ion size. This simple modification does not only enforce counterion saturation, it also leads to a nonmonotonic dependence of the differential capacitance on the surface potential.[37] Fedorov and Kornyshev[35] have pointed out that the approach has been introduced independently by multiple authors starting already in 1942;[38] it leads to the modified Poisson–Boltzmann equation[34]

$$\Psi_e'' = \kappa_e^2 \frac{\sinh \Psi_e}{1 - \phi_0(1 - \cosh \Psi_e)} \tag{11}$$

where $\phi_0 = 2a^3 n_0$ is the volume fraction of the salt ions in the bulk. The inset of Figure 3 shows the local counterion volume fraction $a^3 n_+ \sim 1/(1 + 2e^{\Psi_e}(1 - \phi_0)/\phi_0)$ calculated from the solution of eq 11 with the boundary conditions $\Psi_e'(0) = -4\pi l_e \sigma_e/e$ and $\Psi_e(x \to \infty) = 0$. The two sets of curves in the inset correspond to the two surface charge densities $\sigma_e/e = -1/\text{nm}^2$

DOI: 10.1021/acs.langmuir.5b02389
Langmuir 2015, 31, 11477−11483

(solid lines) and $\sigma_e/e = -2/\text{nm}^2$ (dashed lines). Similar to our present model, the lattice gas GC model predicts counterion saturation that is largely independent of the bulk salt concentration. However, the model does not produce a Stern layer with its ion depletion zone, large magnitude of the surface potential $\Psi_e(0)$, and capacitor-like properties close to the surface.

The GCS model of the EDL places a Stern adsorption plane at distance d_{Stern} away from the charged surface. In addition to the fixed charge density σ_e at the surface, the Stern adsorption plane is assumed to carry a surface charge density σ_{Stern} that originates from ion adsorption. The GCS model does not specify the origin of the ion adsorption; it may reflect exclusively electrostatic attraction or a combination of electrostatic interactions and nonelectrostatic binding.[27] It is also common to assume a uniform dielectric constant ϵ_{Stern} within the Stern layer (that is, in the region $0 \le x \le d_{\text{Stern}}$), which may be significantly smaller than the dielectric constant of bulk water, ϵ_W. Mathematically, the dimensionless electrostatic potential according to the GCS model is

$$\Psi_e(x) = \begin{cases} \Psi_e(d_{\text{Stern}}) - \dfrac{4\pi l_e}{\epsilon_{\text{rel}}}\dfrac{\sigma_e}{e}(x - d_{\text{Stern}}) \\ 2\ln\left[1 - \dfrac{2}{1 + e^{\kappa_e(x-d_{\text{Stern}})}\coth\dfrac{\Psi(d_{\text{Stern}})}{4}}\right], \end{cases} \tag{12}$$

where the upper line describes the parallel-plate capacitor in the region $0 \le x \le d_{\text{Stern}}$ and the lower line the diffuse ion layer for $x \ge d_{\text{Stern}}$. Also, $\epsilon_{rel} = \epsilon_{\text{Stern}}/\epsilon_W$ is the relative dielectric constant within the Stern layer, and

$$\Psi_e(d_{\text{Stern}}) = 2\,\text{arsinh}\left[\frac{2\pi l_e}{\kappa_e e}(\sigma_e + \sigma_{\text{Stern}})\right] \tag{13}$$

is the dimensionless electrostatic potential at the Stern adsorption plane. Note that σ_{Stern} is a phenomenological parameter that can in principle take on any value, but the two limiting cases of significance are $\sigma_{\text{Stern}} = -\sigma_e$ and $\sigma_{\text{Stern}} = 0$. The former reduces the problem to that of a simple parallel-plate capacitor, the Helmholtz model, while the latter implies no specific ion adsorption at the Stern plane. In Figure 4 we compare the prediction of the present GC model with hydration repulsion to the GCS model of the EDL. The blue solid and dashed lines show $\Psi_e(x)$ for $l_h = 0.4$ nm with and without cation−cation hydration repulsion included (these are the same blue curves as already shown and discussed in the upper diagram of Figure 2). Recall that we identify the position $x = d_{\text{Stern}}$ of the counterion concentration maximum $n_+(d_{\text{Stern}})$ with the position of the Stern layer; $x = d_{\text{Stern}} = 0.77$ nm for the case displayed in Figure 4 (marked by the dashed vertical line). To compare our present model with the GCS model of the EDL, we also plot in Figure 4 the potential $\Psi_e(x)$ according to eq 12, derived for $\sigma_e/e = -1$ nm^2, $\kappa_e^{-1} = 1$ nm, and $\epsilon_{\text{rel}} = 1$. The five different solid lines correspond to different values of the surface charge density σ_{Stern} at the Stern plane: $\sigma_{\text{Stern}} = -\sigma_e$, $\sigma_{\text{Stern}} = -0.75\sigma_e$, $\sigma_{\text{Stern}} = -0.5\sigma_e$, $\sigma_{\text{Stern}} = -0.25\sigma_e$, and $\sigma_{\text{Stern}} = 0$ (from top to bottom). Note there is a discontinuous change in slope for $\Psi_e(x)$ at $x = d_{\text{Stern}}$ for all $\sigma_{\text{Stern}} \neq 0$. When $\sigma_{\text{Stern}} = -\sigma_e = 1\ e/\text{nm}^2$, the potential profile $\Psi_e(x)$ corresponds to that of a parallel-plate capacitor. The surface potential $\Phi(0) = \Psi_e(0) \times 0.025$ V (plotted as a function of σ_{Stern} in the inset of Figure 4)

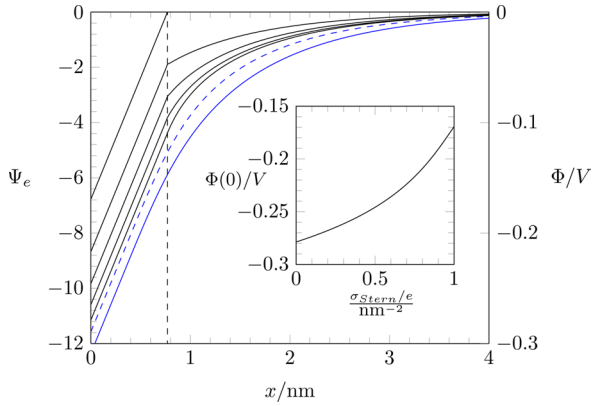

Figure 4. The two blue lines (one solid and one dashed) replot the potential profiles from the upper diagram in Figure 2 for $l_h = 0.4$ nm. The vertical dashed line marks the position $x = d_{\text{Stern}} = 0.77$ nm of the Stern plane (see the blue bullet in the lower diagram of Figure 2). The five black solid lines show $\Psi_e(x)$ according to eq 12 (the GCS model) for $\sigma_e/e = -1/\text{nm}^2$, $\kappa_e^{-1} = 1$ nm, $\epsilon_{\text{rel}} = 1$, and different values of the surface charge density σ_{Stern} at the Stern layer: $\sigma_{\text{Stern}} = -\sigma_e$, $\sigma_{\text{Stern}} = -0.75\sigma_e$, $\sigma_{\text{Stern}} = -0.5\sigma_e$, $\sigma_{\text{Stern}} = -0.25\sigma_e$, and $\sigma_{\text{Stern}} = 0$ (from top to bottom). The surface potential $\Phi(0)$ is plotted in the inset as a function of σ_{Stern}.

is −0.17 V, and the potential outside the Stern layer (that is, for $x > d_{Stern}$) is zero. When $\sigma_{\text{Stern}} = 0$, the surface potential is significantly more negative (−0.28 V) than in the Helmholtz model but remains less negative than the prediction of our present GC model with hydration repulsion (−0.31 V). The origin of this behavior is that the additional repulsive hydration interactions between cations tend to widen the width of the EDL. This renders the surface potential more negative as compared to the GCS model. We note that the similarity of our present model and the GCS model of the EDL also leads to similar values of the differential capacitance $C = \text{d}\sigma_e/\text{d}\Phi(0)$. For the parameters used in Figure 4 (namely, $\sigma_e/e = -1/\text{nm}^2$, $\kappa_e^{-1} = 1$ nm, $\epsilon_{\text{Stern}} = 78$, $d_{\text{Stern}} = 0.77$ nm, and $\sigma_{\text{Stern}} = 0$, which corresponds to the bottom solid black line in Figure 4), we obtain $C = C_{\text{Stern}}C_{GC}/(C_{\text{Stern}} + C_{GC}) = 0.70$ F/m^2, where $C_{\text{Stern}} = \epsilon_{\text{Stern}}\epsilon_0/d_{\text{Stern}} = 0.90$ F/m^2 is the capacitance of a parallel-plate capacitor and $C_{GC} = \epsilon_W\epsilon_0\kappa_e\cosh[\Psi_e(d_{\text{Stern}})/2] = 3.11$ F/m^2 the differential capacitance of the EDL according to the classical GC model. This compares well with our present GC model with hydration repulsion (the solid blue line in Figure 4), for which we obtain $C = 0.72$ F/m^2.

Our final discussion addresses the dielectric constant. The model put forward in the Theory section assumes a uniform dielectric constant throughout the aqueous phase. A more elaborate model could attempt to couple the dielectric constant to the hydration potential or could include dielectric saturation effects,[39,40] but this is beyond the scope of the present work. Instead, we investigate the influence of a fixed drop in the local dielectric constant $\epsilon(x)$ as the distance x to the solid surface decreases. This modification is straightforward to implement in our model by replacing the left-hand side, $\Psi_e''(x)$, of the first equation in eqs 6 by $(\epsilon_{\text{rel}}(x)\Psi_e'(x))'$, where $\epsilon_{\text{rel}}(x) = \epsilon(x)/\epsilon_W$ is the local relative dielectric constant with respect to water. Using MD simulations, Wander and Clark[41] have recently predicted a drop in $\epsilon(0)$ to about 50% of its bulk value $\epsilon(x \to \infty) = \epsilon_W = 78$ at a charged oxide−electrolyte interface; see Figure 5 in ref 41. An exponential decay with a characteristic length $\kappa^{-1} = 0.3$ nm appears to be a reasonable approximation to these

DOI: 10.1021/acs.langmuir.5b02389
Langmuir 2015, 31, 11477−11483

simulation results. A similar exponential decay of $\epsilon(x)$ was also predicted by Podgornik et al.[42] using nonlocal dielectric response theory. We therefore use the function $\epsilon_{rel}(x) = \epsilon_{rel}(0) + (1 - e^{-\kappa x})[1 - \epsilon_{rel}(0)]$ with $\epsilon_{rel}(0) = 0.5$. Figure 5

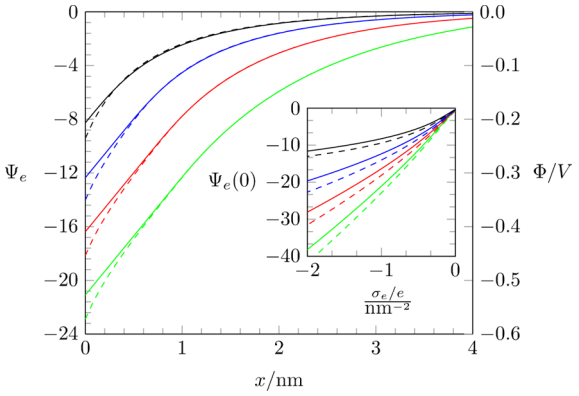

Figure 5. Dimensionless electrostatic potential $\Psi_e(x)$ for $\sigma_e/e = -1/\mathrm{nm}^2$. The solid lines replot the results for uniform dielectric constant, $\epsilon_{rel}(x) \equiv 1$, from the upper diagram in Figure 2, where $l_h = 0.2$ nm (black), $l_h = 0.4$ nm (blue), $l_h = 0.6$ nm (red), and $l_h = 0.8$ nm (green). The dashed lines show the corresponding results for an exponentially decaying dielectric constant with a relative surface value $\epsilon_{rel}(0) = 0.5$. The inset shows the relation between the dimensionless surface potential $\Psi_e(0)$ and the surface charge density σ_e for uniform (solid lines) and exponentially decaying (dashed lines) dielectric constants, the latter with $\epsilon_{rel}(0) = 0.5$.

shows the influence of modifying the dielectric constant close to the surface. The solid lines in Figure 5, which apply to a uniform dielectric constant ($\epsilon_{rel}(x) \equiv 1$), replot results from the upper diagram of Figure 2 (which were calculated for $\sigma_e/e = -1/\mathrm{nm}^2$). The corresponding results with $\epsilon_{rel}(0) = 0.5$ are shown as dashed lines. As expected, the surface potential $\Psi_e(0)$ becomes more negative for the lower dielectric constant near the surface, but the differences between the two models (for $\epsilon_{rel}(0) = 1$ and $\epsilon_{rel}(0) = 0.5$) are minor and do not invalidate the findings of this work. This conclusion remains valid if the surface charge density σ_e is varied; see the inset of Figure 5, which shows the relation between the dimensionless surface potential $\Psi_e(0)$ and surface charge density σ_e for both uniform ($\epsilon_{rel}(0) = 1$, solid lines) and exponentially decaying ($\epsilon_{rel}(0) = 0.5$, dashed lines) dielectric constants. The corresponding relation according to the classical GC model, $\Psi_e(0) = 2\,\mathrm{arsinh}(2\pi l_e \kappa_e^{-1}\sigma_e/e)$, is known as the Grahame equation. The inset of Figure 5 suggests that the relation between $\Psi_e(0)$ and σ_e is strongly influenced by the interionic and ion−surface hydration interactions. For surfaces of equal surface charge density our model predicts the surface potential becomes more negative as the size of the hydrated cation (l_n) increases. This result is qualitatively supported by electrophoretic mobility experiments (colloidal silica in aqueous solutions of LiCl, NaCl, and CsCl) that report on the potential at the start of the diffuse layer (zeta-potentials),[3] but direct comparison with experimentally determined surface potentials is not, at present, possible.

CONCLUSIONS

By simply adding a nonelectrostatic hydration repulsion in the form of a Yukawa potential to the electrostatic interaction inherent in classical Gouy−Chapman theory (the solution of the Poisson−Boltzmann equation), a picture of the EDL that resembles very closely the GCS model emerges naturally. A thin counterion-free region develops at the charged surface whose thickness increases with the effective size of the counterion (crystallographic size plus the thickness of a soft hydration shell). We bound the Stern-like layer by the maximum in counterion concentration, which our model predicts to be physically reasonable and, furthermore, to decrease as the size of the counterion increases. Within the Stern-like region the potential drop to the charged surface is (nearly) linear, again in resemblance to the GCS model of the EDL. We make a direct comparison to the GCS model and conclude that the two models predict effectively the same surface potential only when σ_{Stern} is assumed 0. Finally, we note that the simplicity of our model (both conceptually and mathematically) makes it a convenient tool to fit experimental data or to use it as starting point in further refinements of modeling the EDL. Possible examples regarding the latter include (1) the incorporation of hydration-mediated interactions involving co-ions (instead of only counterions), (2) the addition of oscillations to the hydration potential between mobile ions (which then can capture different ionic hydration states), and (3) the application of the model to different geometries (where a Laplacian replaces the second derivatives in eq 6).

AUTHOR INFORMATION

Corresponding Author

*E-mail: sylvio.may@ndsu.edu (S.M.).

Notes

The authors declare no competing financial interest.

ACKNOWLEDGMENTS

M.A.B. acknowledges the Swiss National Science Foundation for an International Short Visit travel grant to North Dakota State University. G.V.B. acknowledges a doctoral scholarship from CAPES Foundation/Brazil Ministry of Education (Grant No. 9466/13-4).

REFERENCES

(1) Sonnefeld, J. Surface charge density on spherical silica particles in aqueous alkali chloride solutions. *Colloid Polym. Sci.* **1995**, *273*, 932−938.

(2) Porus, M.; Labbez, C.; Maroni, P.; Borkovec, M. Adsorption of monovalent and divalent cations on planar water-silica interfaces studied by optical reflectivity and Monte Carlo simulations. *J. Chem. Phys.* **2011**, *135*, 064701.

(3) Franks, G. V. Zeta potentials and yield stresses of silica suspensions in concentrated monovalent electrolytes: Isoelectric point shift and additional attraction. *J. Colloid Interface Sci.* **2002**, *249*, 44−51.

(4) Kosmulski, M. Positive electrokinetic charge of silica in the presence of chlorides. *J. Colloid Interface Sci.* **1998**, *208*, 543−545.

(5) Tobias, D. J.; Hemminger, J. C. Chemistry. Getting specific about specific ion effects. *Science* **2008**, *319*, 1197−1198.

(6) Kunz, W. *Specific Ion Effects*; World Scientific: Singapore, 2010; Vol. *325*.

(7) Boström, M.; Williams, D.; Ninham, B. Specific ion effects: Why DLVO theory fails for biology and colloid systems. *Phys. Rev. Lett.* **2001**, *87*, 168103.

(8) Zhang, Y.; Cremer, P. S. Interactions between macromolecules and ions: The Hofmeister series. *Curr. Opin. Chem. Biol.* **2006**, *10*, 658−663.

(9) Stern, O. The theory of the electrolytic double shift. *Z. Elektrochem. Angew. Phys. Chem.* **1924**, *30*, 508−516.

DOI: 10.1021/acs.langmuir.5b02389
Langmuir 2015, 31, 11477−11483

(10) Larson, I.; Attard, P. Surface charge of silver iodide and several metal oxides. Are all surfaces Nernstian? *J. Colloid Interface Sci.* **2000**, *227*, 152−163.
(11) Pilon, L.; Wang, H.; d'Entremont, A. Recent advances in continuum modeling of interfacial and transport phenomena in electric double layer capacitors. *J. Electrochem. Soc.* **2015**, *162*, A5158−A5178.
(12) Lyklema, J. *Fundamentals of Interface and Colloid Science: Soft Colloids*; Academic Press: New York, 2005; Vol. *5*.
(13) Lue, L.; Zoeller, N.; Blankschtein, D. Incorporation of nonelectrostatic interactions in the Poisson-Boltzmann equation. *Langmuir* **1999**, *15*, 3726−3730.
(14) Biesheuvel, P.; van Soestbergen, M. Counterion volume effects in mixed electrical double layers. *J. Colloid Interface Sci.* **2007**, *316*, 490−499.
(15) Bhuiyan, L.; Outhwaite, C. Comparison of exclusion volume corrections to the Poisson-Boltzmann equation for inhomogeneous electrolytes. *J. Colloid Interface Sci.* **2009**, *331*, 543−547.
(16) Alijó, P.; Tavares, F.; Biscaia, E., Jr. Double layer interaction between charged parallel plates using a modified Poisson-Boltzmann equation to include size effects and ion specificity. *Colloids Surf., A* **2012**, *412*, 29−35.
(17) López-García, J. J.; Horno, J.; Grosse, C. Poisson-Boltzmann description of the electrical double layer including ion size effects. *Langmuir* **2011**, *27*, 13970−13974.
(18) Kalcher, I.; Dzubiella, J. Structure-thermodynamics relation of electrolyte solutions. *J. Chem. Phys.* **2009**, *130*, 134507.
(19) Burak, Y.; Andelman, D. Hydration interactions: Aqueous solvent effects in electric double layers. *Phys. Rev. E: Stat. Phys., Plasmas, Fluids, Relat. Interdiscip. Top.* **2000**, *62*, 5296.
(20) Ruckenstein, E.; Manciu, M. The coupling between the hydration and double layer interactions. *Langmuir* **2002**, *18*, 7584−7593.
(21) Manciu, M.; Ruckenstein, E. Specific ion effects via ion hydration: I. Surface tension. *Adv. Colloid Interface Sci.* **2003**, *105*, 63−101.
(22) Bohinc, K.; Shrestha, A.; Brumen, M.; May, S. Poisson-Helmholtz-Boltzmann model of the electric double layer: Analysis of monovalent ionic mixtures. *Phys. Rev. E* **2012**, *85*, 031130.
(23) Marcelja, S.; Radic, N. Repulsion of interfaces due to boundary water. *Chem. Phys. Lett.* **1976**, *42*, 129−130.
(24) Verwey, E. J. W.; Overbeek, J. T. G. *Theory of the Stability of Lyophobic Colloids*; Elsevier: New York, 1948.
(25) Israelachvili, J. N.; McGuiggan, P. M. Forces between surfaces in liquids. *Science* **1988**, *241*, 795−800.
(26) Dill, K. A.; Truskett, T. M.; Vlachy, V.; Hribar-Lee, B. Modeling water, the hydrophobic effect, and ion solvation. *Annu. Rev. Biophys. Biomol. Struct.* **2005**, *34*, 173−199.
(27) Parsons, D. F.; Boström, M.; Nostro, P. L.; Ninham, B. W. Hofmeister effects: Interplay of hydration, nonelectrostatic potentials, and ion size. *Phys. Chem. Chem. Phys.* **2011**, *13*, 12352−12367.
(28) Kielland, J. Individual activity coefficients of ions in aqueous solutions. *J. Am. Chem. Soc.* **1937**, *59*, 1675−1678.
(29) Kalcher, I.; Schulz, J. C. F.; Dzubiella, J. Ion-specific excluded-volume correlations and solvation forces. *Phys. Rev. Lett.* **2010**, *104*, 097802.
(30) Shen, J.-W.; Li, C.; van der Vegt, N. F.; Peter, C. Transferability of coarse grained potentials: Implicit solvent models for hydrated ions. *J. Chem. Theory Comput.* **2011**, *7*, 1916−1927.
(31) Mirzoev, A.; Lyubartsev, A. P. Effective solvent mediated potentials of Na+ and Cl- ions in aqueous solution: Temperature dependence. *Phys. Chem. Chem. Phys.* **2011**, *13*, 5722−5727.
(32) Duignan, T. T.; Parsons, D. F.; Ninham, B. W. A continuum solvent model of ion-ion interactions in water. *Phys. Chem. Chem. Phys.* **2014**, *16*, 22014−22027.
(33) Gur, Y.; Ravina, I.; Babchin, A. J. On the electrical double layer theory. II. The PoissonBoltzmann equation including hydration forces. *J. Colloid Interface Sci.* **1978**, *64*, 333−341.
(34) Borukhov, I.; Andelman, D.; Orland, H. Steric effects in electrolytes: A modified Poisson-Boltzmann equation. *Phys. Rev. Lett.* **1997**, *79*, 435−438.
(35) Fedorov, M. V.; Kornyshev, A. A. Ionic liquid near a charged wall: Structure and capacitance of electrical double layer. *J. Phys. Chem. B* **2008**, *112*, 11868−11872.
(36) Shapovalov, V. L. The interaction of electric field and hydrostatic pressure in an electrical double layer: A simple first principle model that accounts for the finite sizes of counterions. *J. Colloid Interface Sci.* **2015**, *454*, 187−191.
(37) Kilic, M. S.; Bazant, M. Z.; Ajdari, A. Steric effects in the dynamics of electrolytes at large applied voltages. I. Double-layer charging. *Phys. Rev. E* **2007**, *75*, 021502.
(38) Bikerman, J. Structure and capacity of electrical double layer. *Philos. Mag.* **1942**, *33*, 384−397.
(39) Booth, F. The dielectric constant of water and the saturation effect. *J. Chem. Phys.* **1951**, *19*, 391−394.
(40) Wang, H.; Varghese, J.; Pilon, L. Simulation of electric double layer capacitors with mesoporous electrodes: Effects of morphology and electrolyte permittivity. *Electrochim. Acta* **2011**, *56*, 6189−6197.
(41) Wander, M. C.; Clark, A. E. Structural and dielectric properties of quartz-water interfaces. *J. Phys. Chem. C* **2008**, *112*, 19986−19994.
(42) Podgornik, R.; Cevc, G.; Žekš, B. Solvent structure effects in the macroscopic theory of van der Waals forces. *J. Chem. Phys.* **1987**, *87*, 5957−5967.

DOI: 10.1021/acs.langmuir.5b02389
Langmuir 2015, 31, 11477−11483